

## **MODELING AND CORRECTING ILLUMINATION INHOMOGENEITY OVER MULTIPLE DLP ILLUMINATION INTENSITIES FOR BETTER FABRICATION ACCURACY**

Saroj Subedi\*, Henry Oliver Tenadooah Ware\*

\*Department of Mechanical and Aerospace Engineering, North Carolina State University,  
Raleigh, NC, 27695

### **Abstract**

Within custom Digital Light Processing (DLP) systems, various small issues either in the optical assembly or with the DMD can lead to non-uniform illumination at the curing interface. This inhomogeneity leads to inaccurate dimensions of fabricated features over the full print area. To remedy this in our system, we have explored the relationship between LED output illumination, divided the illuminated area into a regional mesh, measured the light intensity and grayscale values over the mesh to obtain region-specific grayscale mask adjustments for illumination-leveling. This process involves producing grayscale mask by quantifiably balancing the light intensity values over build area and thus obtaining more uniform printed features. We compared the dimensional accuracy of features printed using full white pixel value images for 250 $\mu$ m features and those obtained using illumination-leveling grayscale processed images. Our results demonstrate the effectiveness of our method to obtain dimensionally accurate features, thanks to the achieved uniform illumination.

### **1. Introduction**

Digital Light Processing (DLP) technology has gained significant attention in the three-dimensional (3D) printing industry due to its ability to fabricate intricate structures with high precision and speed. This projection-based technology has been widely used in the field of biomedical engineering [1-4], electronic devices [2, 5, 6], soft robotics [7, 8], biomimetic applications [9, 10] and various other sectors due to its high throughput fabrication capabilities and flexibility of the material choices. The fabrication of complicated structures and customizable patterns ascribes to its ability to selectively cure photopolymer resin layer-by-layer in presence of ultraviolet (UV) light in a vat with 2D patterns producing a 3D part [11]. The localized photochemical reaction initiated in response to UV light energy and its propagation to form the fully crosslinked solid polymer from the liquid resin extends its capability to print features with the smallest resolution compared to other 3D printing technologies such as material extrusion-based processes [11, 12]. While the theoretical resolution of the DLP system is equivalent to the pixel size, the achievable resolution depends on the size and density of micromirrors on the digital micromirror device (DMD), optical assembly of the system, light source's wavelength, and the projected size of the image [13]. Although DLP systems are promising to fabricate parts with small resolution, achieving accurate dimensional features can be challenging due to non-uniform illumination at the curing interface. In custom DLP systems, Gaussian distribution of irradiation, the optical assembly and DMD play pivotal roles in determining the quality of illumination [14]. Imperfections in the DMD itself and misalignments in optical assembly can introduce the spatial variation in the light intensity distribution leading to the uneven illumination across the fabrication area inducing the deviations in feature dimensions. The efficiency of fabrication area is also

reduced decreasing the ability to realize the printed parts along the full fabrication area [13]. The fabrication of small features with fewer deviations in dimensions is required in order to achieve the desired functional properties such as achieving superhydrophobicity on the 3D printed surface [9]. Mitigating uneven illumination in custom DLP systems would help achieve thousands of features with more uniform dimensions across the greater fabrication area.

Researchers have investigated various methods to tackle the non-uniform illumination problem in the DLP systems. Several authors have proposed various approaches to optimize the optical design itself to achieve uniform illumination in projection systems or Light Emitting Diode (LED) applications. In one study [15], a gradient-index lens was incorporated to control light distribution and improve uniformity. Another work [16] utilized a fly-eye lens in conjunction with a relay lens group to distribute and homogenize light, ensuring consistent light intensity across the DMD chip. Mathematical modeling and optimization methods were also employed to optimize the design, considering the relationship between the optical energy and design parameters, resulting in improved uniformity [17]. Additionally, a simple source-target luminous intensity mapping method was utilized to design a freeform lens, ensuring a uniform distribution of irradiance on the target surface by manipulating the emitted light from an LED source [18]. Although the researchers have showed improvement in uniformity of light illumination by manipulating the optical design itself, this is complicated and is not likely an available flexibility for the custom DLP systems based on directly commercial vendor projection systems.

Compared to the approaches to alter the optical components of the DLP systems, grayscale method to modulate the light distribution for dimensional accuracies is by far the simplest approach. Montgomery et al. [19] have utilized sub-pixel level grayscale manipulation along the boundaries of 2D images to achieve smoother or round edges from the original sharp pixels improving the surface finish. Zhou et al. [20] used different approach of using a set of mask images, rather than a single image for each layer based on an optimized pixel blending principle which enhanced the XY resolution of mask projection based printing process. In similar work [21], Guven et al. used model-based method to optimize the images by grayscale modification considering the light distribution from all closely related pixels to maintain the accuracy of the voxel. Although these studies have improved the dimensional accuracy of the intended features, they focus on the specific shape like edge, and corner of the features. Not many investigations relevant to reducing the deviations of the XY dimensions of the features printed over the whole fabrication area have been reported. To address the uneven illumination in custom DLP systems, Wang et al. [13] utilized grayscale modification to increase the printing area and reduce the under curing/overcuring of the printed part, however, with a narrow range of power intensities (from  $15.95 \text{ mW/cm}^2$  to  $18.62 \text{ mW/cm}^2$ ). This was achieved by converting the power density color map into 8-bit grayscale images. Our study takes a direct approach by utilizing modelled equations to calculate precise grayscale values for each pixel in order to compensate for uneven illumination. The projection area is investigated with a finer mesh of  $100 \times 100$  pixels over a much broader range from  $1.1 \text{ mW/cm}^2$  to  $11.85 \text{ mW/cm}^2$  compared to mesh of  $160 \times 160$  pixels used in Wang et al.'s work [13]. On top of that, we have validated the achieved uniform illumination by statistically reliable results of reduced deviations in lateral dimensions attained with automated dimensions measurement algorithm.

There are two possible approaches to level the curing energy: 1) adjusting exposure time, or 2) varying light intensity. However, varying exposure time across different spatial locations within a single layer pose challenges. On the other hand, adjusting light intensity through grayscale

modification is more feasible, as the relationship between the light intensity and grayscale value can be experimentally determined. The pixel light intensity follows the Gaussian equation and the effect in lateral width due to superposition of varying light intensity with different grayscale values is described in [20]. This explains the improvement in lateral dimensions due to the uniform leveling in light intensity. However, this approach reduces the overall intensity and increases printing time, making it less suitable for scenarios requiring fast printing. Nevertheless, it proves highly effective for achieving uniform dimensions in small features.

In this work, we present an efficient method of achieving uniform illumination at the fabrication plane of custom DLP systems. We hypothesize that the grayscale mask generated based on the established equations mitigate the inhomogeneous illumination, ultimately reducing the deviations in the dimensions of small features printed across the projection area. First, we establish the equations that describe the relationship between LED excitation power, grayscale values and measured light intensities. Utilizing these equations, we directly generate the custom grayscale mask based on user's specified LED excitation power. Then, the accuracy of the generated mask is verified by comparing it to direct measurements of light intensities. Finally, we demonstrate the improvements in dimensional accuracies of printed features using grayscale modified images compared to printing based on original images. Lastly, our study incorporates automated dimension measurements to ensure statistical reliability.

## 2. Materials and Methods

**2.1 Experimental set up:** The experiment utilized an in-house built bottom-up DLP system as depicted in **Fig. 1a**. The system incorporated a UV light engine (LRS-4KA 4K UV Projector, Keynote Photonics) with a native resolution of  $1528 \times 2716$  pixels, projecting UV light at a wavelength of 385 nm. A 2X magnification lens was employed. The fabrication area at the curing interface was measured to be 28.57 mm  $\times$  16.073 mm, resulting in a theoretical pixel length of 10.52  $\mu\text{m}$ . For in-situ examination of light intensity, a beam splitter (50:50 Non-polarizing Beamsplitter Cube, Thorlabs, USA) splits the light, with 50% directed towards the curing interface and the remaining portion (50%) propagates to the power meter sensor (PS10, Coherent, USA). This configuration facilitated the evaluation of light intensity during the process. Furthermore, the images projected onto the building platform are reflected from the mirror to the camera (ASI294MM Pro, ZWO, China) enabling real-time observation of image projection and printing progress. The z-axis translational stage (X-LSQ075A-E01, Zaber Technologies, USA) was responsible for moving the building platform with user defined printing velocity and layer thickness. Both the building platform and resin container were integrated with Pitch and Yaw manual stages (PY003, Thorlabs, USA) to ensure uniform leveling of the building platform with resin container and coplanarity of curing interface with the focal plane. The projector served as a secondary screen connected to the central Desktop computer via a display port. The LabVIEW programming language was implemented to control z-axis stage and sequentially display the 2D images throughout the printing process.

**2.2 Preparation of Resin Vat and Material:** The resin container in this study was a glass petridish that underwent treatment to reduce the adhesion forces and prevent small feature fractures caused by mechanical elongation. To achieve this, PDMS coating was applied. The prepolymer and curing agent (Sylgard-184 silicone elastomer, Dow Corning, USA) were mixed in the ratio of 20:1 and mechanically stirred for 10 minutes before being poured into the petridish [22]. Bubbles were removed via placement in a vacuum environment, and the mixture was cured at 60°C for 4 hrs

using Vacuum oven (VT6025, Thermo Fisher Scientific, USA). After curing, the resin container was immersed in perfluoro carbon lubricant oil (Krytox GPL 105 oil, Chemours, USA) for 24 hrs ensuring reduced adhesiveness [22]. This process was repeated, and the resin vat was left immersed in oil whenever the resin container was not in use.

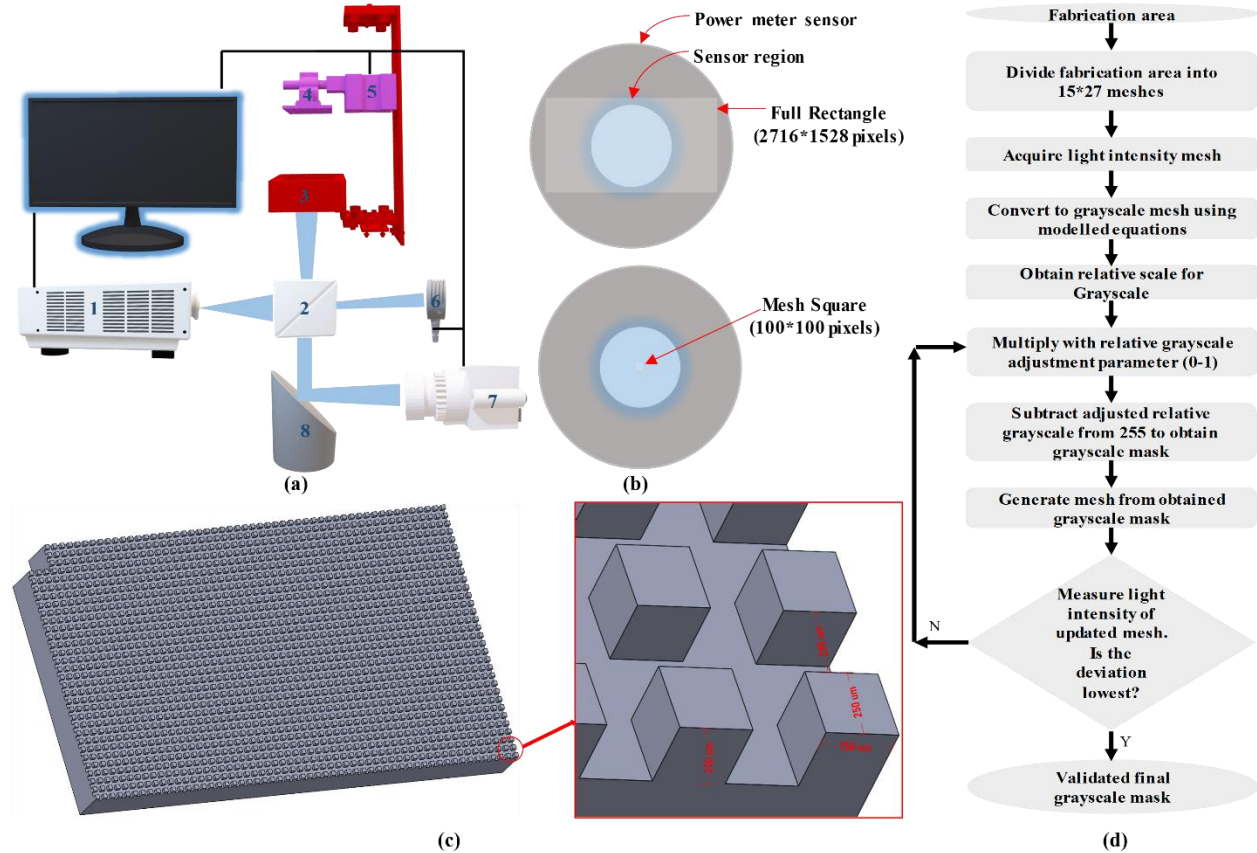


Figure 1 : a) Experimental set up 1. DLP light engine (projector) 2. 50:50 beam splitter 3. Resin vat 4. Building envelope 5. Z-axis translational stage 6. Power meter sensor 7. Camera 8. Reflecting mirror b) Power meter sensor region comparing the projection of full rectangle (2716\*1528 pixels<sup>2</sup>) and mesh square (100\*100 pixels<sup>2</sup>) c) CAD of the part used for the experiment with the dimensions (250 μm) shown in the extended sub-diagram d) Algorithm used to generate the grayscale mask for illumination homogeneity.

The prepolymer used in this experiment was PEGDA700 (Polyethylene Glycol Diacrylate). It was mixed with 2.2% (w/w) of the photoinitiator, Irgacure 819 (Phenylbis(2,4,6-trimethylbenzoyl) phosphine oxide). The combination of this prepolymer and photoinitiator formed the basis for the entire experiment. The depth of penetration ( $D_P$ ) for this prepared material was  $86.88 \mu\text{m}$  while the Critical Energy ( $E_C$ ) required for curing was observed to be  $0.985 \text{ mJ/cm}^2$ . The curing energy for intended layer thickness is optimum across wide range of chosen LED excitation powers, resulting in a smooth and efficient printing process. This material exhibited controllable exposure time, allowing precise control over the curing process. Additionally, it provided excellent shape control during printing. These characteristics make it the ideal material for validating the hypothesis of our study.

**2.3 Grayscale processing of 2D images:** The part design consisted of a solid base of 2 mm thickness and featuring straight square pillars measuring  $250 \mu\text{m}$  in length,  $250 \mu\text{m}$  in height, and

with an edge-to-edge distance of 250  $\mu\text{m}$  (**Fig. 1c**), was designed in CAD software (Solidworks 2021). The resulting design was saved as .stl file, which was subsequently imported and sliced into 2D 8-bit grayscale images using open-source slicer software: ChituBox. The slicing process employed a thickness of 50  $\mu\text{m}$ . Once the 2D projection mask images with full white intensity were obtained, a custom MATLAB program was implemented for further processing. The algorithm converted the grayscale value of each pixel within the 2D images to the corresponding grayscale value specified by the finalized grayscale mask. The processed grayscale 2D images were then saved in a designated directory for utilization during the printing of the samples. The process of obtaining the finalized grayscale mask is detailed in **Section 3.2**.

**2.4 Printing of Samples:** The samples were printed using DLP process based on LABVIEW. For each LED excitation power, two samples were printed for both the original 2D images and final grayscale mask processed 2D images, resulting in a total of 20 samples. A layer thickness of 50  $\mu\text{m}$  was consistently used throughout the experiment. To ensure strong interlayer adhesion, the exposure energy was set at 1.5 times the curing energy required for the given layer thickness. This value(1.5) was experimentally obtained after multiple iterations and decided to be the best for getting a successful print part with optimum interlayer bonding while avoiding significant overexposure. Meanwhile for the samples with grayscale processed images, while the grayscale mask effectively levels the illumination uniformly, the overall light intensity is reduced due to the superposition of lowered grayscales. To compensate for this energy loss, the light intensity corresponding to the lowest grayscale value in the grayscale mask was determined using the modelled equation (*eqn. 1*), and this value was used to calculate the required exposure time (curing energy).

**2.5 Measurement of Dimensions:** The measurement of dimensions was performed by using an optical microscope (SMZ25, Nikon, Japan) for capturing images and using automated algorithm to obtain dimensions. Top-view optical images were captured at a magnification of 3x, focusing on 10 different representative regions of each sample (**Fig. 4c**). To extract the width and height of the pillars, the Canny Edge Detection algorithm was implemented in Python and applied to each sample. The resulting rectangles, representing the detected bounding boxes, were assigned numerical labels and their corresponding height and width values were recorded in an Excel file. Manual inspection was necessary to validate and refine the accuracy of the detected bounding boxes. The instances of eliminated or considered bounding boxes can be referred to **Fig. 4d**. Automating dimension measurement provided numerous benefits, including increased efficiency, reduced human error and the ability to collect a larger number of data points, ultimately resulting in more accurate and robust representation of the results. This algorithm-based approach for data collection ensured consistent and standardized measurements, minimizing the potential human bias. The increased sample size enhanced the statistical validity and generalizability of the findings.

### 3. Modeling and Optimization of Light Intensity Distribution

**3.1 Modelled Linear Relationship:** For our custom DLP system, the LED excitation power ranged from a maximum of 2 W without any device error to a minimum of 0.1 W. To validate the idea of interpolation and cover a sufficient range, a total of five data points were selected including three additional powers at equal intervals (0.524 W, 1.048 W and 1.574 W). The light intensities for each LED excitation power were measured for grayscale values ranging from 0 to 255 at multiples of 5, using power meter sensor at the focal plane. It's important to note here that these

measurements were taken for the original system illumination. The plotted graph of light intensities against the grayscale values (**Fig. 2a**) revealed a clear linear relationship. Furthermore, it is also evident that the slope of the light intensity versus grayscale plot increased with higher LED excitation power (**Fig. 2b**). Additionally, the y-intercept value in a plot of light intensity against grayscale also increased (**Fig. 2c**) with increasing LED excitation power. The y-intercept represents the light intensity when LED is excited, even in the absence of an image or an equivalent grayscale-0 image projection at the focal plane. Although intuitively the intercept should indicate ambient light, the activation of LED at the specific excitation power slightly increased the light intensity value, albeit insignificantly. These linear relationships between three different variables: LED excitation power, grayscale, and light intensity, were modelled (*eqn. 1*) and leveraged to obtain grayscale masks for each LED excitation power.

$$P = m \times GS + c; \text{ where, } m = 0.0219 \times E_p - 0.0001; c = 0.0046 \times E_p + 0.5234 \quad (1)$$

where P represents light intensity ( $\text{mW}/\text{cm}^2$ ), m is slope of line plotted between light intensity and grayscale, GS is grayscale value ranging from 0 to 255, c is the y-intercept; and  $E_p$  denotes the LED excitation power.

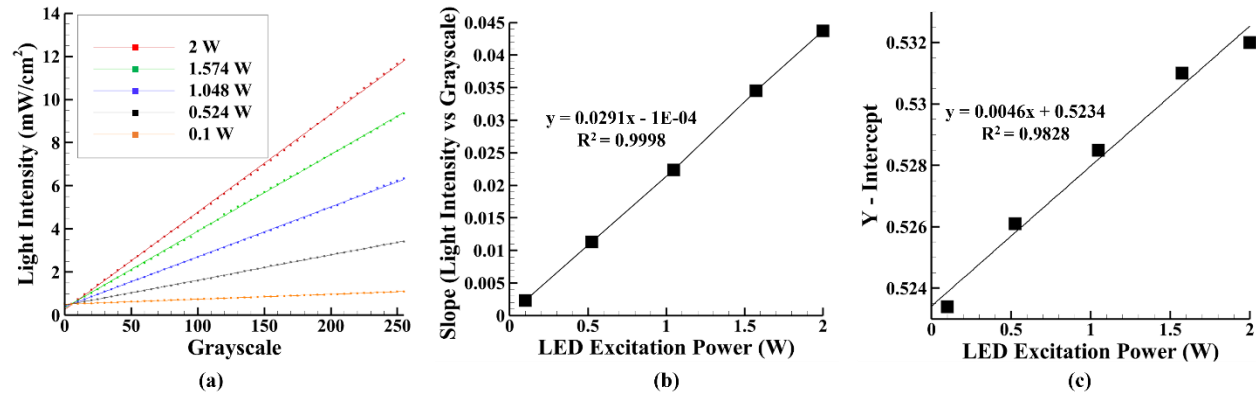


Figure 2 : a) Light intensity ( $\text{mW}/\text{cm}^2$ ) plotted against Grayscale values for five LED excitation powers b) Slope of lines from (a) against LED excitation powers c) Intercept of lines from (a) against LED excitation powers.

**3.2 Generation of Illumination-Leveling Grayscale Mask:** In our DLP system, the fabrication area measures  $28.57 \text{ mm} \times 16.07 \text{ mm}$  equivalent to a pixel resolution of  $2716 \text{ pixels} \times 1528 \text{ pixels}$ . To generate the grayscale mask for illumination leveling, the full pixel array was divided into squares of size  $100 \times 100$  pixels. Using MATLAB, a total of  $15 \times 27$  full white (grayscale-255) squares were generated. The power meter sensor, positioned at the focal plane was mounted on a combination of two linear stages (XR25C, Thorlabs, USA) to enable XY plane measurements of light intensities. The simplified algorithm for generating the grayscale mask is depicted in **Fig. 1c**. Sequentially, the generated full white squares were projected using a custom LABVIEW program, while recording the corresponding light intensity for each square. This process was repeated for LED excitation powers of 2 W, 1.048 W, and 0.1 W, thus, obtaining the respective power meshes. Since this study hypothesizes that the user can eliminate illumination inhomogeneity and work with any LED excitation power without having to obtain power meshes for all LED excitation powers, direct light intensity measurements were performed for only three extreme data points. This approach ensures that the crucial aspects of the LED excitation power range are covered and allows for the validation of the hypothesis. The color map diagram for power meshes for all three LED excitation powers: 2 W, 1.048 W, and 0.1 W are shown in **Fig. 3a**. The maximum difference

between the peak intensity and the minimum intensity within the mesh in the local light intensity is as high as  $2.6023 \text{ mW/cm}^2$  for 2 W LED excitation power,  $1.1204 \text{ mW/cm}^2$  for 1.048 W and  $0.2259 \text{ mW/cm}^2$  for 0.1 W. The power mesh diagrams for 2 W, 1.048 W and 0.1 W (**Fig. 3a**) exhibited similar regions of highest and lowest light intensities. It is crucial to consider the potential deviation from the grayscale mask requirement in the case of low LED excitation power. The differences in light intensity at low power level might suggest that a grayscale mask may not be necessary. However, it is important to emphasize that the curing energy, which determines the exposure time for successful printing remains constant. Consequently, the increased exposure time at lower LED excitation power results in a significant difference in curing energy. Therefore, despite the smaller intensity difference, the use of a grayscale mask remains essential for ensuring accurate and precise curing energy control throughout the printing process.

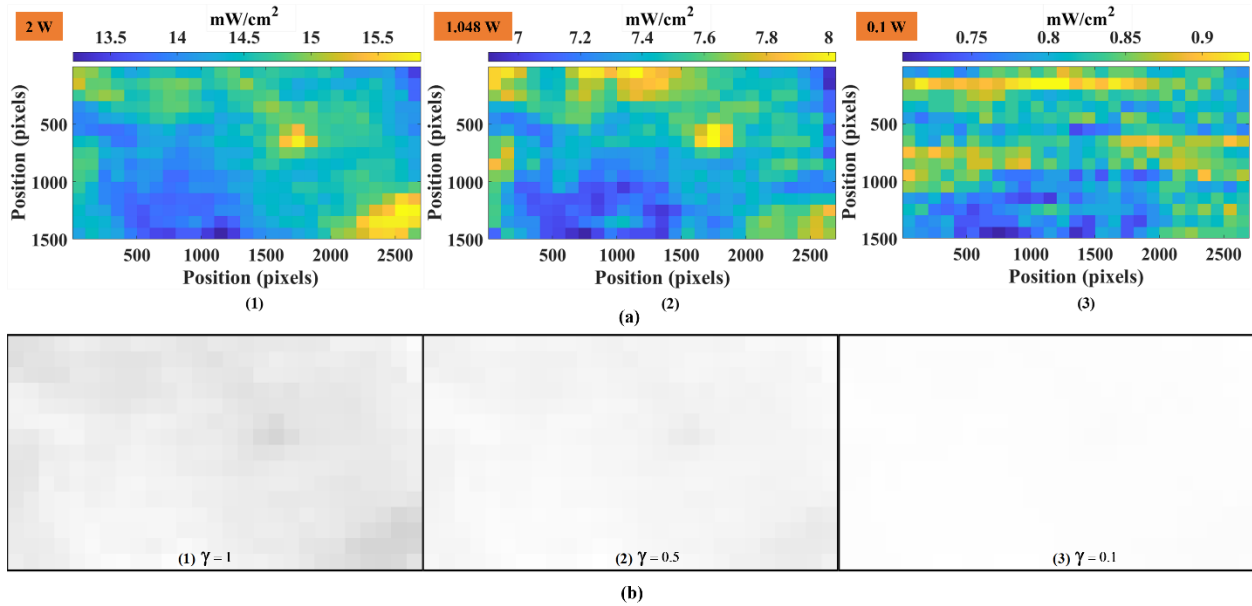


Figure 3: a) Light intensity meshes for 2 W (1), 1.048 W (2), and 0.1 W (3) plotted using MATLAB b) Instance of Grayscale mask for 2 W with relative scale ( $\gamma = 1$  (1),  $\gamma = 0.5$  (2), and  $\gamma = 0.1$  (3))

The underlying concept of this study is based on the assumption of a linear relationship between the light intensities at the resin surface and the LED excitation powers. Although the grayscale mask generated for a single LED excitation power may be ideally applicable to other powers, the slope of the light intensity line plotted against grayscale values varied for each LED excitation power (**Fig. 2a**). This observation indicates that a uniform adjustment in grayscale values for all LED excitation powers will not achieve uniform light intensities. Thus, it becomes necessary to acquire light intensity meshes for at least three different LED excitation powers. One notable significance of our work is the user's flexibility to print using any LED excitation power, enabled by validating the linearity in the obtained light intensity meshes. Using MATLAB, the linear trendline equations and the R-squared values were calculated for the three light intensities corresponding to 0.1 W, 1.048 W, and 2 W at each spatial location. The lowest R-squared value obtained was 0.9882. Out of 405 ( $15 \times 27$ ) data points, 403 data points had R-squared values greater than 0.990, while more than 332 data points had R-squared value greater than 0.995. This demonstrated that the light intensity meshes for any LED excitation power could be generated by

interpolating with linear trendline equations. Adopting this approach, light intensity meshes for 0.524 W and 1.574 W were also obtained.

The conversion of light intensity mesh into a grayscale mesh was achieved through the utilization of modelled equations (*eqn. 1*), which calculated grayscale values based on the given LED excitation power and local intensity. The ultimate goal was to attain a grayscale mask that would ensure uniform illumination. However, it is important to note that the modelled equations were derived from measurements obtained across the entire fabrication area, rather than the localized light intensities. Consequently, the modelled equations facilitated relative adjustments to the grayscale values, rather than the exact adjustments, thereby necessitating the validation of obtained grayscale mask. To compensate for any potential over or under adjustments in grayscale values towards achieving uniform illumination, a relative-scale ( $\gamma$ , ranging from 0 to 1) was introduced. A  $\gamma$  of 1 indicated an excessive adjustment, while a  $\gamma$ -value of 0 indicated an insufficient adjustment. The impact of relative scale on the grayscale mask is shown in **Fig. 3b**. Subsequently, the  $\gamma$  mesh was obtained and subtracted from 255 to yield the final  $\gamma$ -modified grayscale mask. The  $100 \times 100$  pixels squares generated using the  $\gamma$ -modified grayscale mask were randomly projected at different representative locations within the fabrication area, with subsequent measurements of light intensities. The process was repeated iteratively until the discrepancy between the highest and lowest measured light intensities was minimized. After numerous iterations, a relative scale value of 0.5 was found to provide the best fit for the targeted LED excitation powers. Employing this  $\gamma$  relative scale value, finalized grayscale masks were successfully obtained for LED excitation powers of 0.1 W, 0.524 W, 1.048 W, 1.574 W, and 2 W. All of the aforementioned algorithms were programmed in MATLAB.

## 5. Results and Discussions

**5.1 Validation of uniform illumination through direct measurement:** To validate the uniform illumination, a direct measurement approach was employed. Finalized grayscale masks were obtained through multiple iterations by varying the relative scale ( $\gamma$ ), which represents the difference from the minimum value (**Fig. 3b**). Iterations involved multiplying relative grayscale with values in the range of 0.1 to 1. The relative scales 0.1, 0.45, 0.5, 0.55, and 1 were mostly used for iteration. Grayscale processed square meshes of  $100 \times 100$  pixels were generated using the obtained grayscale masks corresponding to different  $\gamma$ -values. These squares were projected at random locations, including the brightest, dimmest, and intermediate regions, and light intensities were experimentally measured at 20 spatial locations. After several iterations, a  $\gamma$ -value of 0.5 was determined to be optimal for all tested LED excitation powers.

The results for experimental validation of uniform illumination with  $\gamma$ -value of 0.5 for three sets of LED excitation power (0.1 W, 1.048 W, and 2 W) are presented in **Fig 5**. Practical challenges, such as fluctuations in power meter sensor measurements and potential discrepancies in positioning the square projection, were encountered, especially near the boundary region of fabrication area. Increased sensitivity of power meter sensor along the boundary might have also contributed to accidental rise in intensity readings due to positioning error. The presence or absence of ambient light by LED activation, contrastively at the center and the boundary region of fabrication area, affected the measured light intensity readings, leading to unintended variations in measurements.

For excitation power of **2 W**, the highest and lowest measured light intensities were narrowed from  $16.26 \text{ mW/cm}^2$  and  $14.52 \text{ mW/cm}^2$ , respectively, for original projection to  $15.37 \text{ mW/cm}^2$  and  $14.52 \text{ mW/cm}^2$  for finalized grayscale processed images. Similarly, for **1.048 W** excitation power the highest and lowest measured intensities were improved from  $8.44 \text{ mW/cm}^2$  and  $7.26 \text{ mW/cm}^2$ , respectively, with original images to  $7.84 \text{ mW/cm}^2$  and  $6.85 \text{ mW/cm}^2$  with finalized grayscale images. In a similar vein, for **0.1 W** excitation power, the highest and lowest intensities exhibited refinements as the original images yielded values of  $0.98 \text{ mW/cm}^2$  and  $0.78 \text{ mW/cm}^2$  while the finalized grayscale processed images showcased improved values of  $0.85 \text{ mW/cm}^2$  and  $0.76 \text{ mW/cm}^2$  for 0.1 W excitation power. The light intensity map and corresponding grayscale mask generation (**Fig. 3**) reveals that the dimmest location maintains a grayscale value of 255. This is in line with the adjustment process, which utilizes the extreme grayscale value (255) to account for the minimum light intensity. As a result, the lowest intensities remained consistent for both the original and grayscale images at **2 W**. Ideally, similar results should have been observed for the intensities at 1.048 W and 0.1 W.

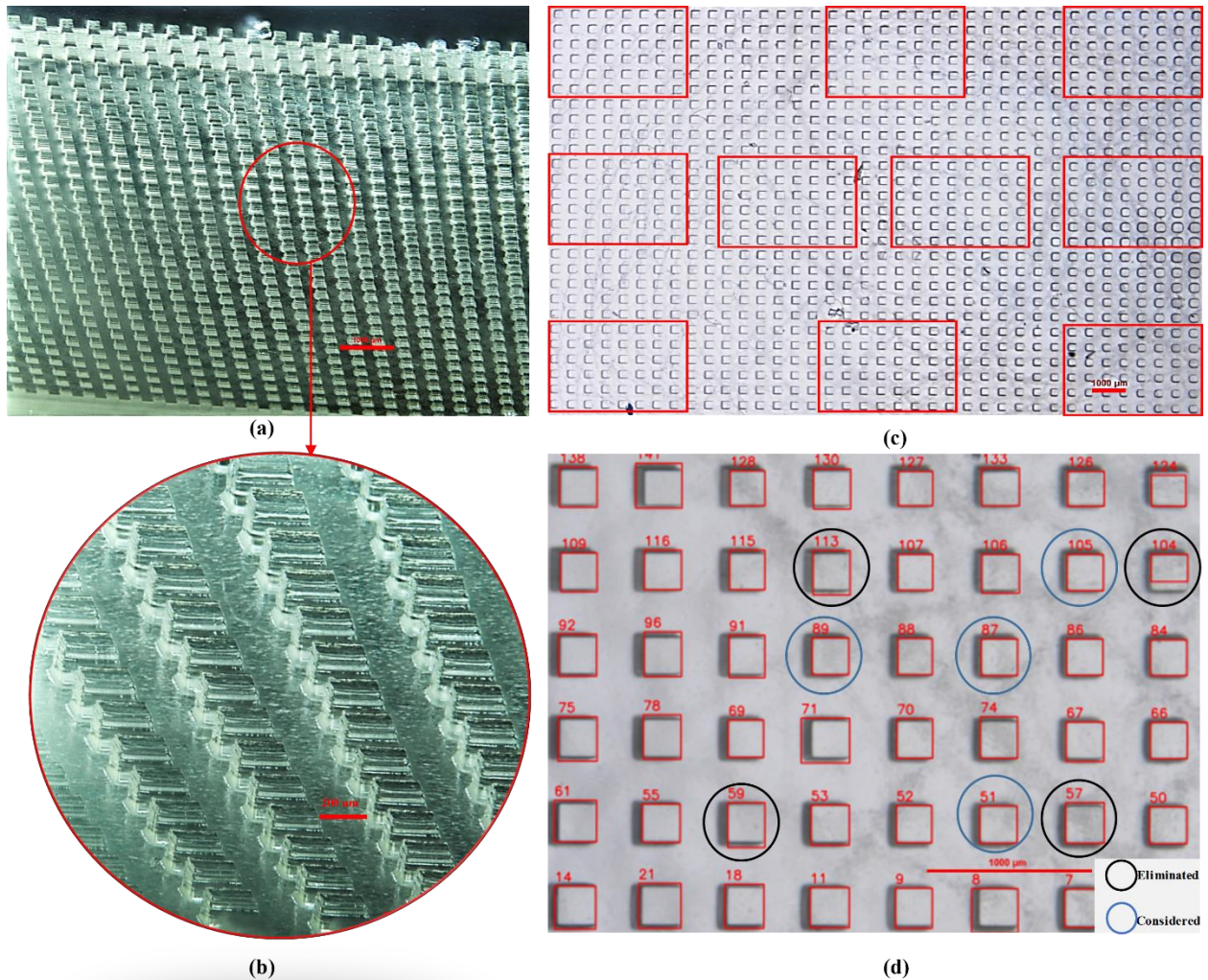


Figure 4: a) Side view of printed sample at 1x (scale:  $1000 \mu\text{m}$ ) and b) at 3x (scale:  $200 \mu\text{m}$ ) c) Top-view (scale:  $1000 \mu\text{m}$ ) of printed sample showing all regions used for dimensions measurements d) Samples of eliminated and considered dimensions obtained using Canny Edge Detection algorithm in Python (scale :  $1000 \mu\text{m}$ )

However, minor deviations in the lower intensities occurred due to experimental errors and fluctuations in power meter sensor readings. In retrospect, it is possible to choose a grayscale value lower than 255 for dimmest mesh during the illumination adjustment process while still achieving uniform illumination. However, this would result in a decrease in the overall light intensity necessitating an increase in exposure time consequently elevating the total printing time. Similarly, the standard deviations were lowered from 0.51 mW/cm<sup>2</sup> to 0.25 mW/cm<sup>2</sup>, 0.36 mW/cm<sup>2</sup> to 0.26 mW/cm<sup>2</sup>, and 0.060 mW/cm<sup>2</sup> to 0.026 mW/cm<sup>2</sup> respectively for **2W**, **1.048 W**, and **0.1 W**, respectively (Fig. 5a).

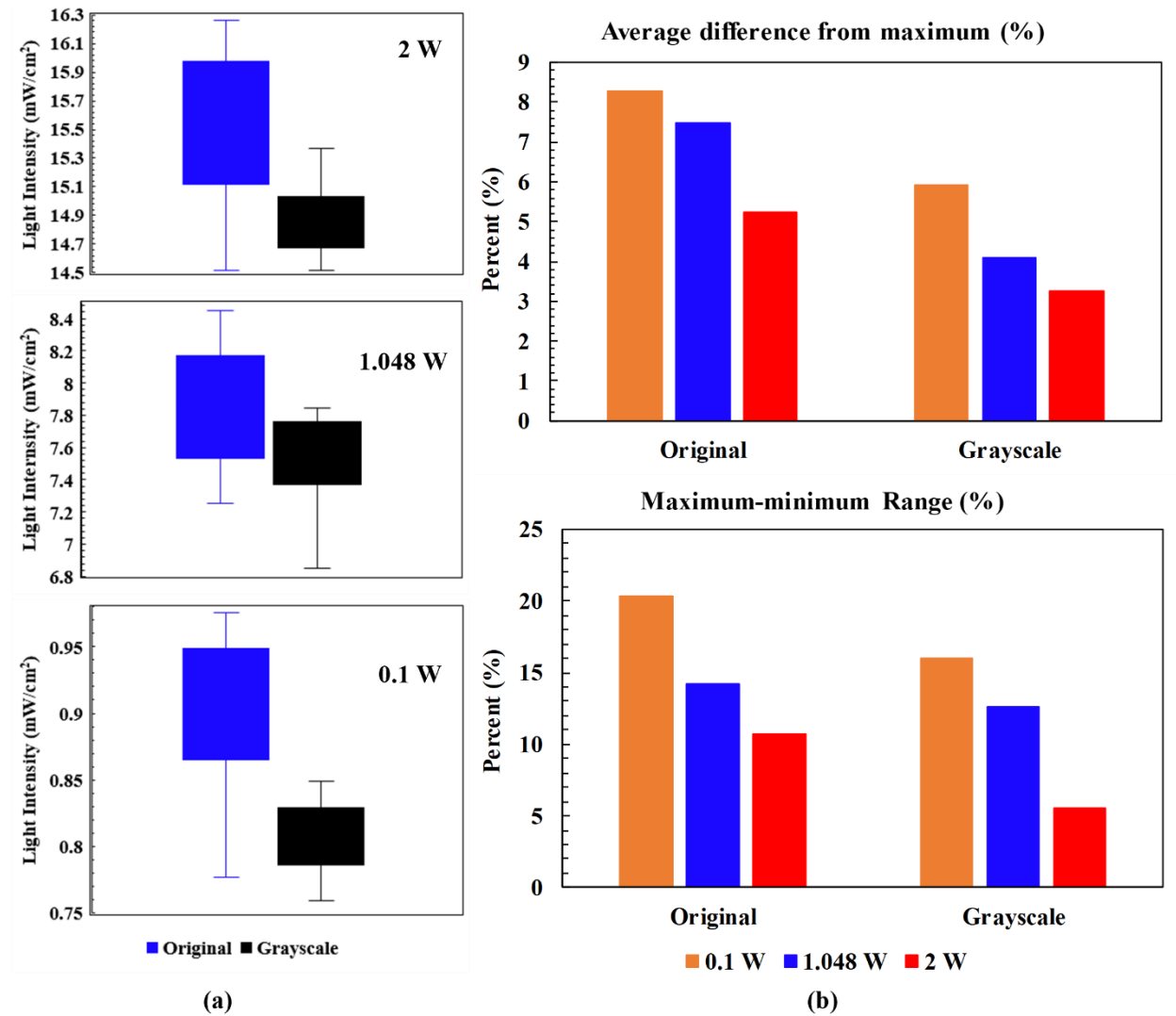


Figure 5 : Experimental Validation of uniform illumination a) Standard deviation of original illumination and uniform illumination obtained after grayscale processing b) Comparison of average difference from Maximum and Maximum-minimum Range in percentage.

The improvement in uniform illumination was also demonstrated by calculating the mean of average differences from maximum and calculating maximum-minimum ranges as well. The percentage-based differences for the average difference from the maximum were improved from 5.23%, 7.5%, and 8.28% (original images) to 3.25%, 4.1%, and 5.94% (grayscale processed images) for **2 W**, **1.048 W** and **0.1 W** LED excitation powers respectively. Moreover, the

maximum-minimum ranges were reduced from 10.72%, 14.23%, and 20.37% to 5.53%, 12.67%, and 15.96% respectively. The observed phenomenon of histogram plots exhibiting an increase, as the LED excitation power is decreased, can be attributed to the growing significant effect of fluctuations in power meter sensor readings and because the percentage of the lower value tends to become more pronounced. Notwithstanding, these results validate the approach adopted in this study for achieving more uniform illumination.

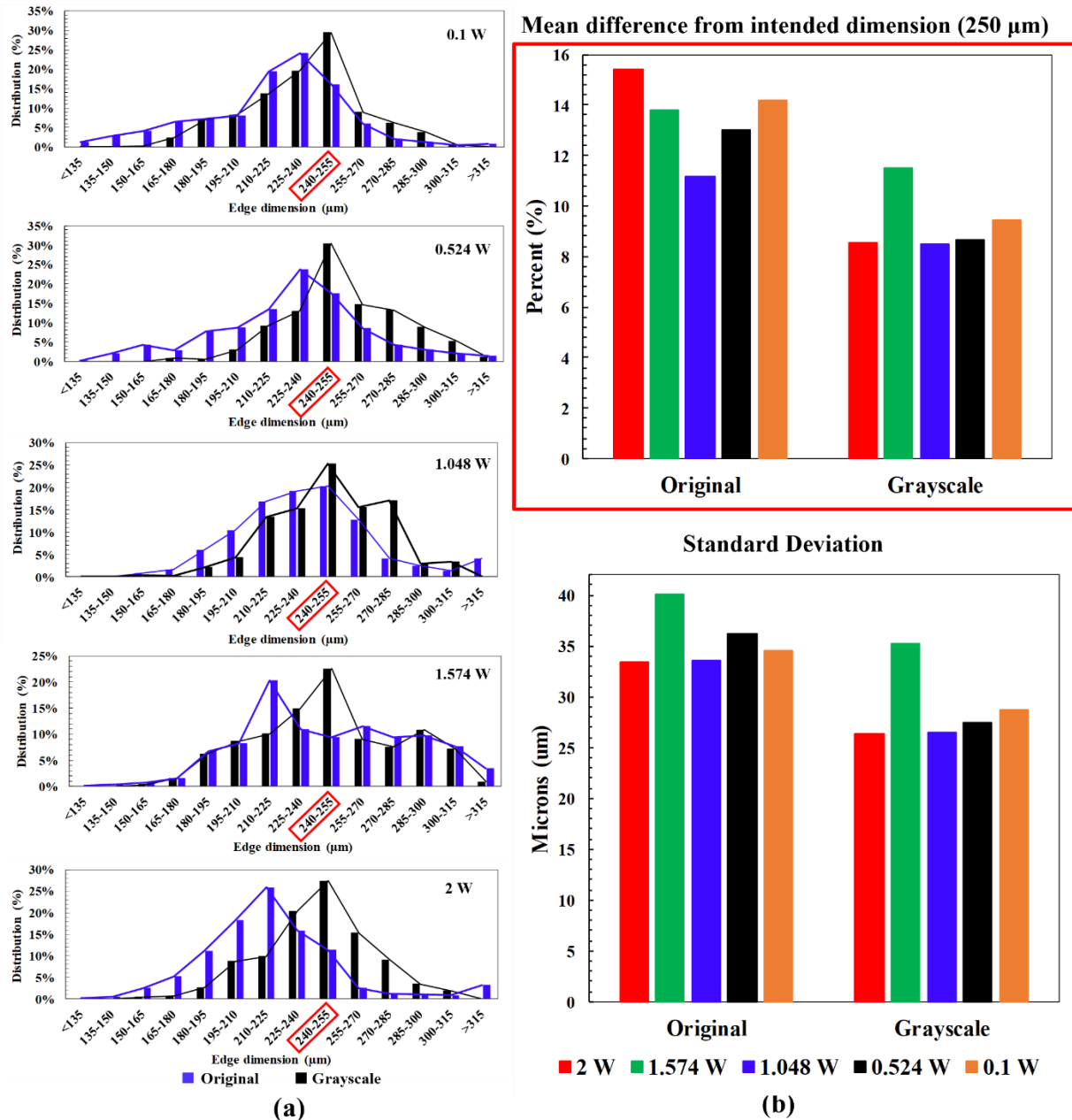


Figure 6: Comparison of dimensional results using original full white, and grayscale processed images a) Histogram comparison. The red highlighted section indicates the intended design dimension of the pillars. b) Comparison of mean from the intended dimension (250 µm) and standard deviation

**5.2 Validation of uniform illumination through printing samples:** Once all the optical images of testing regions were acquired, the canny edge detection algorithm as described in **Section 4.2** was applied to each image. Subsequently, the detected edges underwent manual inspection and filtering, and the finalized width and height measurements were recorded in Excel sheets. Since the intended dimension was a square from the top view, the average of width and height was taken and treated as the single data point for the dimension. These average dimensions were used to interpret the results in **Fig 6**. **Fig 6a** illustrates the histogram comparison, highlighting the shift in the dimensional results attributed to the uniform illumination achieved through grayscale mask processed images. Notably, the histogram are plotted based on percentage of the data samples for optimal comparison.

The peak of the histogram (number of data samples falling within the given range) shifted from 225-240  $\mu\text{m}$  range to 240-255  $\mu\text{m}$  range for **0.1 W**, from 225-240  $\mu\text{m}$  to 240-255  $\mu\text{m}$  for **0.524 W**, from 210-225  $\mu\text{m}$  to 240-255  $\mu\text{m}$  for **1.574 W**, and from 210-225  $\mu\text{m}$  to 240-255  $\mu\text{m}$  for **2 W**. For unifying comparison, the intended dimensions of the pillar widths were 250 $\mu\text{m}$ . The histogram for grayscale-modified illumination for **1.048 W** showed 2 peaks, with the highest being in the 240-255 $\mu\text{m}$  bin, and a smaller peak at the 270-280  $\mu\text{m}$  bin. Although the peak for **1.048 W** did not shift from 240-255  $\mu\text{m}$  range, an increment in the peak indicated the improvement in the results. Assuming the intended dimension of the pillars within the range of 240  $\mu\text{m}$  to 270  $\mu\text{m}$ , the area under the curve demonstrated improvement for all sets of LED excitation power indicating an increased number of datasets falling within that region. The observed trimming of the extreme dimensions (**Fig. 6a**) in the printed features when using grayscale-processed images provided empirical evidence supporting the effectiveness of the approach adopted in this study in reducing the deviation in feature dimensions. This finding underscores the potential of grayscale processing technique as a means to enhance the accuracy and precision of printed features in additive manufacturing processes.

An alternative approach to interpreting the results involved calculating the average difference from the intended dimension (250  $\mu\text{m}$ ) and standard deviation (**Fig. 6b**). The average difference from intended dimension rather than the extremes was chosen for calculation, as the aim was to center the results towards the designed dimension. The measured mean difference from the intended dimension reduced from 15.41%, 13.78%, 11.15%, 13.02%, and 14.2% (original pure-white image values) to 8.56%, 11.51%, 8.49%, 8.63%, and 9.44% (grayscale processed images) for **2W**, **1.574 W**, **1.048 W**, **0.524 W**, and **0.1 W** respectively. Furthermore, a similar improvement in standard deviation was observed, as the standard deviations for the original images were 33.42  $\mu\text{m}$ , 40.10  $\mu\text{m}$ , 33.58  $\mu\text{m}$ , 36.17  $\mu\text{m}$ , and 34.59  $\mu\text{m}$  compared to 26.34  $\mu\text{m}$ , 35.28  $\mu\text{m}$ , 26.52  $\mu\text{m}$ , 27.49  $\mu\text{m}$ , and 28.69  $\mu\text{m}$  with the grayscale modified images for **2W**, **1.574 W**, **1.048 W**, **0.524 W**, and **0.1 W** respectively.

Although our study encountered challenges in perfectly mitigating illumination inhomogeneity, there are avenues for further improvement. Using a higher precision power meter sensor with reduced fluctuations, and maintaining consistency in intensity readings, could yield more reliable light intensity meshes. Additionally, ensuring data collection at a consistent focal plane is crucial, as even slight variations can significantly impact light intensity readings. Automating the experimental set up by integrating a power meter sensor with programmable translational stages would enable real-time light intensity measurements. This automated system could be linked with the grayscale mask algorithm, allowing for automatic projection at different

grayscale levels until the light intensity closely matches the lowest value in the original light intensity mesh. Also, projecting mesh squares that crosses mesh element boundaries by a few pixels could even increase the quality of acquired light intensity mesh data by making it more continuous rather than discretized data. This approach minimizes human errors and offers a promising path towards achieving optimal homogeneous illumination. Furthermore, while our study focused on the impact of uniform illumination on lateral dimensions, it would be valuable to explore the effects of achieved illumination homogeneity on layer dimensions and accumulated energy dosage. Investigating these aspects could provide insights into the improvements that can be attained through this approach.

## **6. Conclusions**

In this study, the hypothesis was presented that addressing the issue of inhomogeneous illumination at the fabrication plane could lead to improvements in the lateral (X-Y planar) dimension of printed features. The proposed approach involved generating a full projection area illumination-leveling grayscale mask based on the modeled relationship between LED excitation power, light intensity, and grayscale values. By utilizing this relationship, a grayscale mask was generated for a user-defined LED excitation power, and the sliced 2D images were processed accordingly for printing. The effectiveness of achieving uniform illumination was experimentally verified by directly measuring light intensities using the grayscale mask mesh. To validate the improvement in the dimensions of the features, square pillars of 250  $\mu\text{m}$  dimensions were printed using grayscale mask for five representative LED excitation powers. The dimensions of the printed features were measured using a custom automated algorithm for boundary detection. The results demonstrated that the extreme dimensions were reduced, and a greater number of data samples fell within the intended dimension range.

The successful mitigation of uneven illumination in custom DLP systems showcases the practicality to achieving dimensional uniformity in small-scale printed features and enables reliable printing over the entire projection area. Future research directions could involve automating the correction process with a combination of linear stages and a power meter sensor which would read the local intensity values, generate grayscale values until the desired uniform intensity is achieved, and perform validation. Additionally, exploring the characterization of various photopolymer resins other than PEGDA would extend the applicability of this approach. Improvement in dimensional uniformity should be expected using the approach from this work for any other photopolymer resin, however, the extent of improvement could vary based on photosensitivity, and curing kinetics. The incorporation of machine learning algorithms to measure dimensions and enhance the statistical significance of the results is also a promising avenue. Furthermore, investigating the impact of this approach on the improvement of dimensions due to accumulated dosage of multiple layers would provide valuable insights for further advancements.

## References

1. Li, Y., et al., *Theoretical prediction and experimental validation of the digital light processing (DLP) working curve for photocurable materials*. Additive Manufacturing, 2021. **37**.
2. Han, T., et al., *3D Printed Sensors for Biomedical Applications: A Review*. Sensors, 2019. **19**(7).
3. Mo, X., et al., *Advances in digital light processing of hydrogels*. Biomedical Materials, 2022. **17**(4).
4. Zhang, J., et al., *Digital Light Processing Based Three-dimensional Printing for Medical Applications*. International Journal of Bioprinting, 2020. **6**(1): p. 12-27.
5. Wei, T.S., et al., *3D Printing of Customized Li-Ion Batteries with Thick Electrodes*. Advanced Materials, 2018. **30**(16).
6. Mu, Q.Y., et al., *Digital light processing 3D printing of conductive complex structures*. Additive Manufacturing, 2017. **18**: p. 74-83.
7. Mao, Y.Q., et al., *Sequential Self-Folding Structures by 3D Printed Digital Shape Memory Polymers*. Scientific Reports, 2015. **5**.
8. Kuang, X., et al., *Grayscale digital light processing 3D printing for highly functionally graded materials*. Science Advances, 2019. **5**(5).
9. Yang, Y., et al., *3D-Printed Biomimetic Super-Hydrophobic Structure for Microdroplet Manipulation and Oil/Water Separation*. Advanced Materials, 2018. **30**(9).
10. Li, X.J., et al., *3D-Printed Cactus-Inspired Spine Structures for Highly Efficient Water Collection*. Advanced Materials Interfaces, 2020. **7**(3).
11. Peng, X.R., et al., *Multi-Color 3D Printing via Single-Vat Grayscale Digital Light Processing*. Advanced Functional Materials, 2022. **32**(28).
12. Montgomery, S.M., et al., *A reaction-diffusion model for grayscale digital light processing 3D printing*. Extreme Mechanics Letters, 2022. **53**.
13. Wang, Y.C., D. Xue, and D.Q. Mei, *Projection-Based Continuous 3D Printing Process With the Grayscale Display Method*. Journal of Manufacturing Science and Engineering-Transactions of the Asme, 2020. **142**(2).
14. Li, Y., et al., *High-fidelity and high-efficiency additive manufacturing using tunable pre-curing digital light processing*. Additive Manufacturing, 2019. **30**.
15. Rui, D.W., et al., *Optical design in illumination system of digital light processing projector using laser and gradient-index lens*. Optical Engineering, 2012. **51**(1).
16. Jiang, H.N., et al., *Projection optical engine design based on tri-color LEDs and digital light processing technology*. Applied Optics, 2021. **60**(23): p. 6971-6977.
17. Bai, X.Q., X.L. Jing, and N.F. Liao, *Design method for the high optical efficiency and uniformity illumination system of the projector*. Optics Express, 2021. **29**(8): p. 12502-12515.
18. Chen, J.J., et al., *Freeform lens design for light-emitting diode uniform illumination by using a method of source-target luminous intensity mapping*. Applied Optics, 2015. **54**(28): p. E146-E152.
19. Montgomery, S.M., et al., *Pixel-Level Grayscale Manipulation to Improve Accuracy in Digital Light Processing 3D Printing*. Advanced Functional Materials, 2023. **33**(17).
20. Zhou, C., and Yong Chen., *Additive manufacturing based on optimized mask video projection for improved accuracy and resolution* Journal of manufacturing processes 14.2 (2012): 107-118., 2012.
21. Guven, E., Y. Karpat, and M. Cakmakci, *Improving the dimensional accuracy of micro parts 3D printed with projection-based continuous vat photopolymerization using a model-based grayscale optimization method*. Additive Manufacturing, 2022. **57**.
22. Zhang, Y., et al., *Continuous 3D printing from one single droplet*. Nature Communications, 2020. **11**(1).